Single fluorogen imaging reveals spatial inhomogeneities within biomolecular condensates

Authors: Tingting Wu[1,2], Matthew R. King[2,3], Mina Farag[2,3], Rohit V. Pappu[2,3*], Matthew D. Lew[1,2*]

Affiliations:

[1] Department of Electrical and Systems Engineering, Washington University in St. Louis, James F. McKelvey School of Engineering, Washington University in St. Louis, St. Louis, MO 63130, USA

[2] Center for Biomolecular Condensates, James F. McKelvey School of Engineering, Washington University in St. Louis, St. Louis, MO 63130, USA

[3] Department of Biomedical Engineering, Washington University in St. Louis, James F. McKelvey School of Engineering, Washington University in St. Louis, St. Louis, MO 63130, USA

e-mail: pappu@wustl.edu; mdlew@wustl.edu

Abstract

Recent investigations have suggested that biomolecular condensates are viscoelastic materials. This implies that material properties of condensates are governed by internal microstructures. Furthermore, computations show that the internal organization in protein condensates is spatially inhomogeneous, featuring hub-and-spoke-like percolated networks of molecules. Here, we test these predictions using imaging of single fluorogenic dyes that are turned-on in response to specific chemical microenvironments. We deployed Nile blue (NB), Nile red (NR), and merocyanine 540 (MC540) for epifluorescence and single-molecule localization microscopy imaging of condensates formed by intrinsically disordered, low-complexity domains of proteins. Imaging with NB reveals internal environments that are uniformly hydrophobic, whereas NR shows preferential binding to hubs that are more hydrophobic than the surrounding background within condensates. Finally, imaging with MC540 suggests that interfaces of condensates are unique chemical environments. Overall, the high spatiotemporal resolution and environmental sensitivity of single-fluorogen imaging reveals spatially inhomogeneous organization of molecules within condensates.

Main Text

Biomolecular condensates provide spatial and temporal control over biochemical reactions in cells [1]. Proteins with intrinsically disordered regions (IDRs) such as prion-like low complexity domains (PLCDs) and arginine-glycine-rich (RG-rich) regions tend to be prominent drivers of different types of protein-based condensates [2,3]. These IDRs are biological instantiations of linear associative polymers featuring cohesive motifs known as stickers that are interspersed with solubility determining spacers [4]. Stickers form reversible physical crosslinks with one another, whereas spacers modulate sticker-sticker interactions and the coupling between phase separation and percolation [5]. Here, percolation refers to the formation of system-spanning networks [6], and is the more precise and general term for gelation [5].

Recent investigations of material properties suggest that condensates, including those formed by simple systems such as PLCDs and RG-rich IDRs, are viscoelastic materials [7-11]. In general, viscoelastic materials feature complex, spatially inhomogeneous network-like internal

structures [12]. The short-time behaviors of viscoelastic fluids are elastic whereas their long-time behaviors are viscous. The converse is true for viscoelastic solids [12].

Computational studies have made headway in describing the spatial organization of molecules within condensates [10,13,14]. In recent work, Farag et al.,[10] used a coarse-grained lattice-based model to simulate the phase behavior of the wild-type PLCD from the protein hnRNP-A1, which we refer to hereafter as A1-LCD [15]. The simulations uncovered a spatially inhomogeneous network-like structure that is akin to that of a small-world graph featuring a hub-and-spoke organization with hubs being defined by collections of molecules forming intermolecular physical crosslinks [10]. The degree of spatial inhomogeneity and connectivity within small-world network topologies are governed by the valence of stickers and the differences in interaction strengths between different stickers and spacers [10]. In this work, we asked if these predictions could be tested directly using experiments.

The network-like organization of protein molecules within viscoelastic condensates has been uncovered using cryo-electron tomographic reconstructions for condensates formed by the full-length yeast prion protein Sup35 [16]. This work revealed a microstructure with a regular mesh size. However, most condensates, especially those that are viscoelastic fluids rather than solids, are likely to feature an assortment of mesh-like structures whose sizes vary spatially and temporally [17]. This makes it challenging to use the conventional tools of structural biology [8] for mapping the sequence- or composition-specific internal structures of condensates. Quantifying the time-averaged structure within a condensate requires a technique with multiscale resolution and with sufficient sensitivity to detect transient as well persistent interactions between molecules. This requires the ability to discriminate rare and relatively weak signals from strong signals that stem from the average ensemble. Single-molecule spectroscopy of fluorescently labeled macromolecules is useful for quantifying the dynamics of small numbers of individual proteins [18,19]. However, these methods cannot be scaled up to characterize spatial inhomogeneities that are the defining hallmarks of viscoelastic materials.

In this work, we combine fluorogenic probes [20-22] with single-molecule imaging [23-28] to uncover the organization and dynamics of molecules within condensates. Fluorogenic molecules are environmentally sensitive probes that change their emission properties such as fluorescence intensities, emission spectra, and fluorescence lifetimes, in response to changes in chemical environments [20-22,29-31]. Here, we report results from measurements of protein condensates formed by A1-LCD [2,32] and the RG-rich IDR from the protein DDX4 [3,33]. Three fluorogens, namely, Nile blue (NB), Nile red (NR) [20,21], and merocyanine 540 (MC540)[22] were used as separate probes of the internal structures and dynamics of protein condensates. Notably, the proteins themselves are not chemically modified by the dyes. Instead, the fluorogens are free to move around [34]. These fluorogens are dark in aqueous solutions, even when pumped with an excitation laser. As the probes diffuse through solution, they can partition into less hydrophilic environments or bind to locally hydrophobic regions, thereby causing an increase in fluorescence quantum yield (**Fig. 1a**).

Heterogeneities within condensates revealed by three fluorogens

In bulk epifluorescence imaging, we found that each probe exhibits a fluorescence signal from within condensates that is different from the signal within the coexisting dilute solution. However, each of the dyes sees these environments from a different perspective (**Fig. 1b-1d**). The fluorescence intensity of NB is uniform throughout each condensate, indicating a uniform distribution of binding sites for NB (**Fig. 1b**). NR fluorescence, however, is clustered into

microscale "hubs" that are twice as bright as their background (**Fig. 1c**). Hubs are observable in condensates that form on and above the coverslip (**See Supplementary Video 1**). These data suggest that NR fluoresces in response to specific molecular architectures within each condensate. Finally, MC540 fluoresces strongly at the interface between the dense and dilute phase of each condensate. This implies that the interface is a unique environment (**Fig. 1d**). Uniqueness of interfaces can arise from proteins adopting different conformations or relative arrangements at the interface [22]. Indeed, this was a feature that was predicted by recent computations [10].

We observed nonuniform spatial organization within condensates even as they adsorbed onto the coverslip. Fluorogenic probes tracked internal rearrangements as the condensates deformed (**Fig. 1e-g**): NB fluorescence is uniform across each condensate; clusters of NR move apart from one another; and the strong MC540 fluorescence at the condensate interface dissolves into a more uniform distribution as the condensates adsorb to and wet the coverslip (**Fig 1d** and **Extended Data Fig. 2a, 2b)**. Although MC540 has negligible impact on bulk phase separation (**Extended Data Fig. 3**), our epifluorescence images revealed that MC540 induces heterogeneities in condensates even at low, ~1.7 μM, concentrations (**Extended Data Fig. 2c**). Therefore, for the remainder of the study, we focused on data gathered using NB and NR.

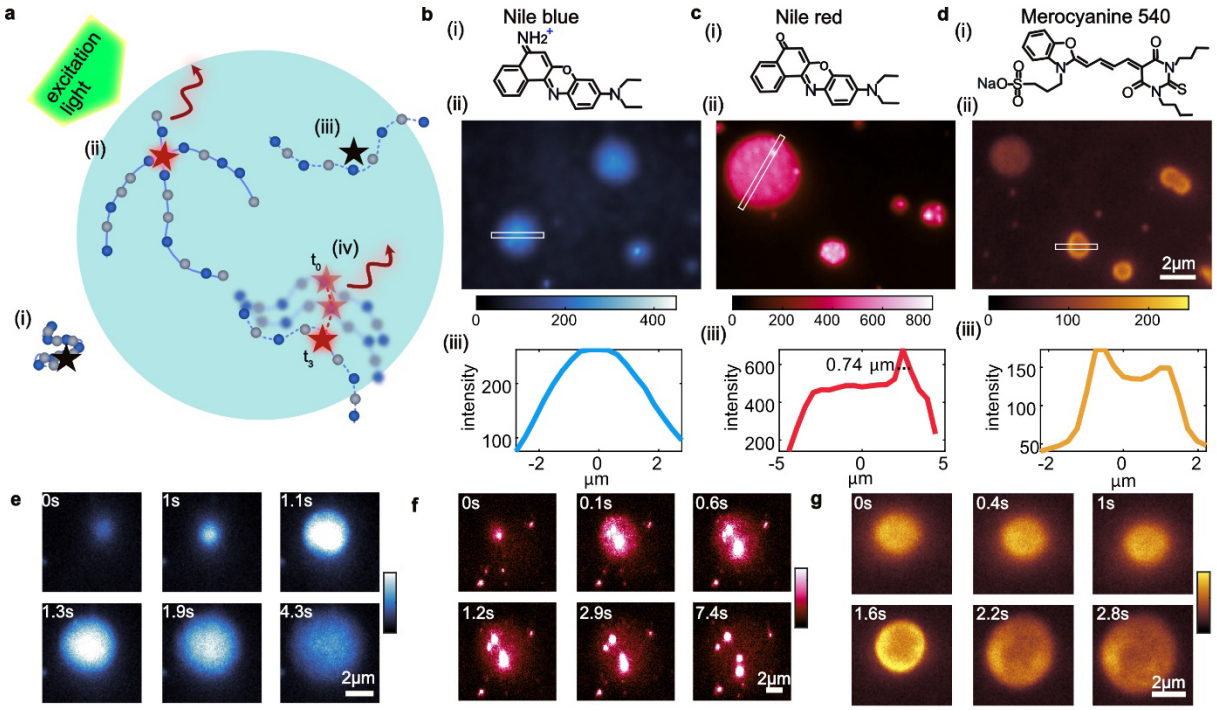

Fig. 1: Epifluorescence imaging shows that fluorogenic probes sense chemical environments inside biomolecular condensates from different perspectives. a. As fluorogenic probes (stars) randomly translate through solution, they encounter various chemical environments formed by the low-complexity domain of the hnRNPA1 protein (A1-LCD, chains of blue and gray circles) in the dilute phase (white space) or in the condensate (large blue circle). In response, they either (i,iii) remain dark (black stars) or (ii,iv) become fluorescence emitters (red arrows). This (ii,iv) affects their velocities. b,c,d, Imaging A1-LCD condensates using **b**. Nile blue (NB), **c**. Nile red (NR), and **d**. merocyanine 540 (MC540). (i) Chemical structures of the fluorogens. (ii) Typical condensates as viewed by

epifluorescence microscopy. (iii) Fluorescence intensity profiles along the long axis of white box shown in (ii). **e**,**f**,**g**, Dynamic wetting of the glass coverslip by proteins condensates, as perceived by **e**. NB, **f**. NR, and **g**. MC540.

To compare how the fluorogenic probes perceive internal structures with varying sensitivity, we imaged single condensates sequentially using NB and NR (see Methods). Both NB and NR exhibit microscale hubs in similar spatial locales that rise above an otherwise uniform background fluorescence (**Fig. 2a, 2b**). However, the hubs uncovered using NR are always higher in intensity when compared to those accessible to NB. Further, we always observed additional hubs with NR when compared to NB.

The excitation and emission spectra of NR and NB are known to shift towards blue wavelengths with decreasing solvent polarity [35]. To ascertain if there are any spatial inhomogeneities in solvent polarity within the condensates, we imaged the dyes within condensates in two separate wavelength regions using orange (593 ± 23 nm) and red (676 ± 18 nm) bandpass filters (**Fig. 2c, 2d**). We detected mostly uniform NR and NB fluorescence within the red emission window. These images indicate that the microscale hubs imaged using NR and NB are only weakly associated with polar environments. However, in the orange emission window, the background fluorescence virtually disappears while the hubs for both NR and NB dyes persist. These data suggest that the NR and NB hubs are foci of non-polar chemical environments within the condensates.

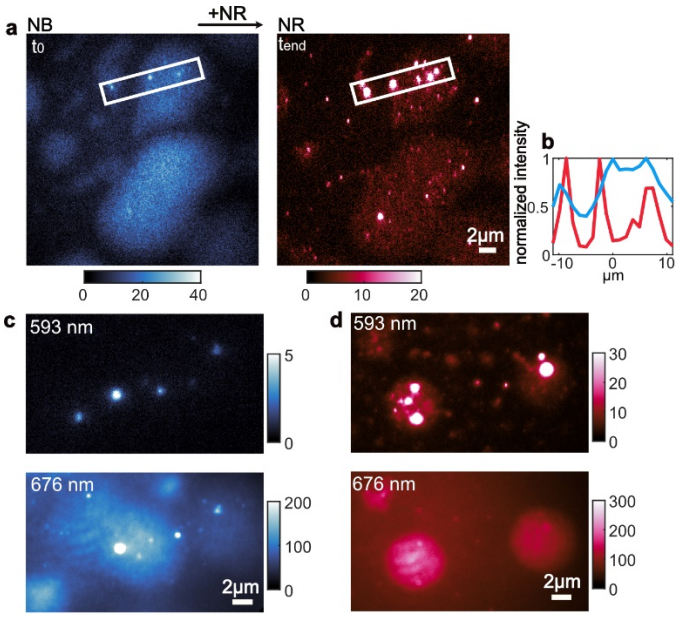

Fig. 2: Both the fluorescence intensity and solvatochromic shift of NB and NR are correlated with inhomogeneous spatial organization of molecules within biomolecular condensates. a, Epifluorescence images of condensates collected using NB (left), and then adding NR (right). **b.** Fluorescence intensity profiles (blue: NB, red: NR) along the long axis of the white boxes shown in (**a**). **c,d,** Epifluorescence microscopy of biomolecular condensates collected using two emission windows (top: 593±23 nm and bottom: 676±18 nm) each for (**c**) NB and (**d**) NR. For both probes, fluorescence collected in the orange emission window (593 nm) was excited using a 532-nm laser, and fluorescence collected in the red emission window (676 nm) was excited using a 637-nm laser.

It has been established that aromatic residues inside A1-LCD function as stickers that enable physical crosslinks between proteins [2,32]. Conversely, charged, and polar residues interspersed between the stickers act as spacers [2,32]. Considering these data, we propose that the

microscale hubs uncovered using NR and NB are direct readouts of networked molecules formed via intermolecular physical crosslinks among collections of aromatic stickers.

Nanoscale heterogeneities within condensates observed by SM imaging

Diffraction-limited epifluorescence microscopy has insufficient spatial resolution (~200 nm) to map the nanoscale chemical environments within each condensate. We leveraged the diffusion and transient binding of NB, NR, and MC540 [34,36] as a photo-switching ("blinking") mechanism for super-resolved single-molecule localization microscopy (SMLM) [37-40]. As individual probes diffuse through solution, they are dark until they bind to hydrophobic sites, and we measured the locations of the resulting fluorescence flashes [23]. Accumulating the positions of many blinking events yielded SMLM reconstructions that map the internal structure within each condensate with nanoscale resolution and single-molecule sensitivity (see Methods and **Supplementary Video 2**).

Super-resolution images of single condensates showed that both NR and NB exhibit non-uniform localization patterns that persist for several minutes (**Fig. 3a, 3b**). To quantify this heterogeneity using single-molecule blinking (**Fig. 3c**), we calculated the excess variance within each condensate. If a fluorogenic probe has a uniform probability of blinking across the entire condensate, we would expect its localization density to be Poisson-distributed [41]; this behavior would yield an excess variance of zero (**Extended Data Fig. 4**). Remarkably, five condensates sequentially imaged by NB and NR all show larger than expected variances with a mean value of 1.3 ± 0.8 (std. dev., 2.1×10^4 localizations/condensate on average). Thus, SMLM shows large and significant variations in single molecule blinking thereby implicating spatially diverse interactions between proteins within each condensate (**Fig. 3c**).

In accord with epifluorescence imaging (**Fig. 1**), which shows inhomogeneities on the scale of the optical diffraction limit, the super-resolution images of NR also showed inhomogeneities, albeit on scales that are below the diffraction limit. We refer to this scale as the nanoscale. To quantify the relative affinities of NR and NB for binding to what we refer to as "nanoscale hubs" within a condensate, we measured the relative proportion of localizations that are spatially clustered (**Fig. 3d, 3e)**. For each localization, we compared the local density to the surrounding density and assigned a cluster coefficient [42,43]; molecules with cluster coefficients above a certain threshold are classified as being clustered (**Fig. 3d**, see Methods). For the five condensates imaged by NR and NB, 27% ± 3% of NR molecules and 13% ± 4% of NB molecules were clustered. This indicates that clustering happens twice as often with NR when compared to NB dyes.

Next, we quantified the similarities and differences between the spatial inhomogeneities mapped by NR and NB using coordinate-based correlation or CBC (see Methods) [44,45]. CBC between two SMLM datasets quantifies how the localization density distribution around each emitter in one SMLM dataset is correlated, uncorrelated, or anti-correlated with the localization density distribution at the corresponding position in the other SMLM dataset. CBC scores will be −1 for perfectly anticorrelated distributions, 0 for uncorrelated distributions, and +1 for perfectly correlated distributions. For both NR and NB images, regions with few localizations are mostly uncorrelated (median±1 quartile score of 0.16 ± 0.39 for NB and 0.07 ± 0.40 for NR, **Fig. 3f**). However, regions containing a high density of NR and NB localizations are highly correlated with one another, as indicated by large positive CBC scores (median ±1 quartile score of 0.99 ± 0.003 for NB and 0.94 ± 0.12 for NR, **Fig. 3f**, **Extended Data Fig. 5**). This relationship also holds for condensates imaged by MC540 and NB (**Extended Data Fig. 6**).

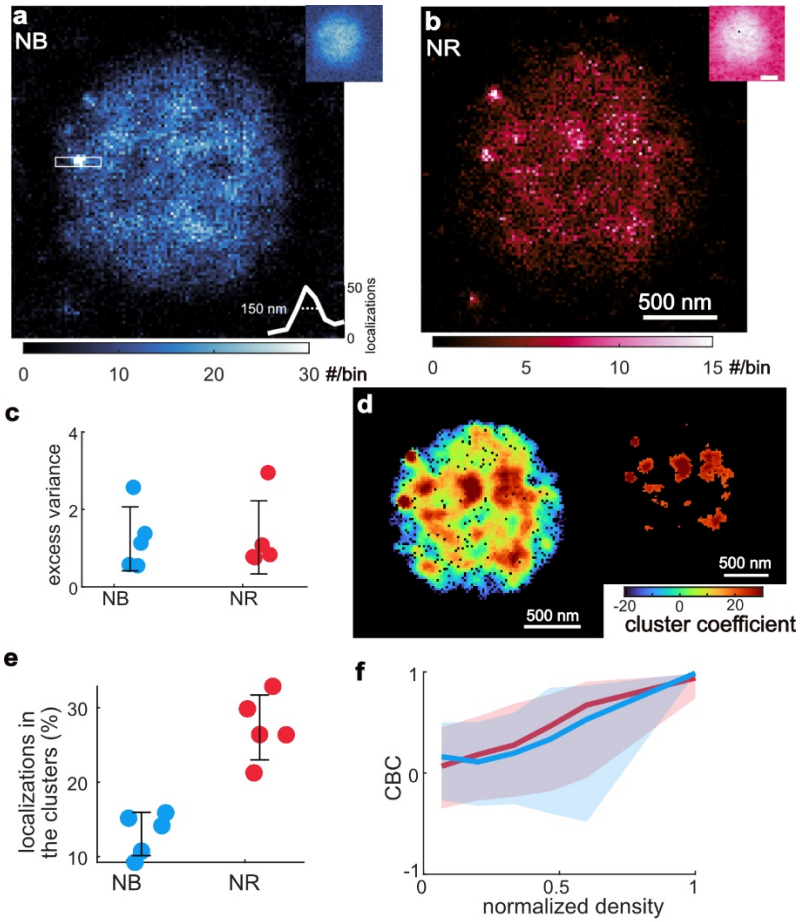

Fig 3: Single-molecule localization microscopy (SMLM) of NB and NR reveals that molecules are organized into nanoscale clusters within biomolecular condensates. a,b, SMLM images of a single condensate collected using (**a**) NB and (**b**) NR. Top inset: epifluorescence image; bottom inset: localization profile along the long axis of the while box shown in (**a**). Color bars: number of single molecules within each 20 nm × 20 nm bin. **c,** Quantifying the heterogeneous binding and activation of NB (blue) and NR (red) within five condensates using excess variance (see Methods). Larger excess variances represent greater heterogeneities in the blinking statistics of fluorogenic probes within a condensate; zero excess variance represents uniform blinking statistics throughout the condensate. **d,** Condensate imaged by NR in **b** color-coded by cluster coefficient (Methods). Inset: emitters that have a cluster coefficient larger than 20. **e,** Percentages of single-molecule localizations that are spatially clustered for five condensates. **f,** Coordinate-based correlation (CBC, See Methods) between NB and NR localizations in **a** and **b**, plotted as a function of localization density. Data are plotted from the perspective of NB (blue) or of NR (red). Solid lines: median; shaded area: 25th-75th percentiles.

Overall, the data suggest that A1-LCD proteins form hydrophobic hubs within the condensates, thereby facilitating the binding and fluorogenic activation of single NR, NB, and MC540 molecules. Favorable binding on the timescale of ~10 ms camera frames and fluorescence activation correlated with non-polar chemical environments are necessary for mapping hubs with single-molecule sensitivity and nanoscale resolution.

Nanoscale dynamics in condensates quantified by single-molecule tracking

Single-molecule imaging shows that nanoscale hubs within each of the condensates disappear from one location and reappear at nearby locations. These events occur on timescales of

minutes (**Supplementary Video 3,4**). To probe dynamics inside condensates, we tracked the movements and fluorescence burst durations of individual probes (**Supplementary Video 5**). We report the burst duration t_b, which is correlated with the amount of time a molecule spends in a fluorescence-promoting environment, and the magnitude of the velocity, which measures the displacement of a fluorescing molecule over a 10 ms window (**Fig. 4a**, **Extended Data Fig. 7**). Both parameters vary in response to changes in the chemical environments along the trajectory of the probe. For example, the burst durations of NR range from 10 ms to more than 170 ms (**Fig. 4b**). This heterogeneity is highlighted by reconstructing SMLM images using only single molecules with short burst durations ($t_b \leq 60$ ms, **Fig. 4c**) versus those with long burst durations ($t_b > 60$ ms, **Fig. 4d**). Single molecules with short burst durations are distributed essentially uniformly across the condensate, while hot spots are dominant in the long-burst duration images. This trend is also consistent with condensates imaged by NB (**Extended Data Fig. 8**).

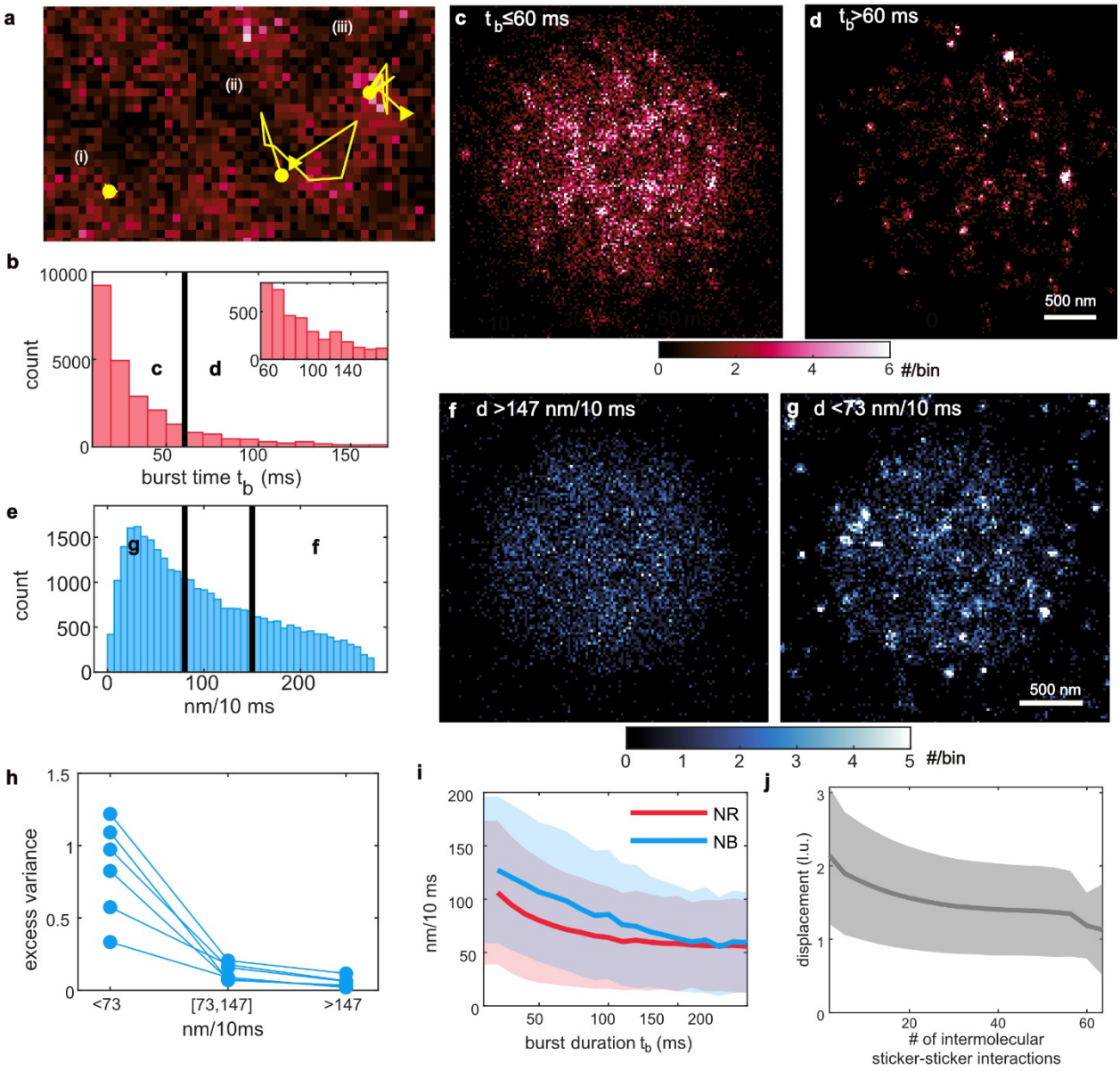

Fig 4: Tracking single-molecule fluorescence burst durations and velocities quantifies inhomogeneous molecular distributions within condensates. a, Single NR exhibit both (i) short and (ii,iii) long burst durations, as well as (ii) high and (iii) low magnitudes of velocities. **b**, Fluorescence burst durations $\mathbf{t_b}$ of NR. **c**,**d**, SMLM images of NR molecules with burst durations (**c**) shorter than 60 ms and (**d**) longer than 60 ms. **e**, NB velocities measured between consecutive camera frames (10 ms exposure time). **f**,**g**, SMLM images of NB molecules with magnitudes of velocities (**f**) larger than 147 nm/10-ms and (**g**) smaller than 73 nm/10-ms. **h**, Excess variance of NB localizations grouped by magnitude of velocity (left: <73 nm/10-ms, middle: between 73/10-ms and 147 nm/10-ms, right: >147 nm/10-ms). Blue lines: excess variance of NB within each condensate. **i**, Velocities of (blue) NB and (red) NR as a function of their fluorescence burst durations. Lines: mean value averaged over 150K trajectories for NB and 129K trajectories for NR; shaded region: ±1 standard deviation. **j**, Magnitude of velocity of each chain within a simulated A1-LCD condensate as a function of the number of intermolecular sticker-sticker interactions it participates in. Measurements originate from a Lattice-based Monte Carlo simulation (LaSSI, See methods). Velocities are measured after 2.5×10^8 total system Monte Carlo moves.

When compared to NR, NB exhibits longer burst durations and larger displacements (**Extended Data Fig. 7**). This weaker affinity to nanoscale hubs enables individual NB probes to explore interactions across longer timescales and larger areas. We separated NB emitters into three categories based on the magnitudes of velocities between consecutive frames (10 ms exposure time, **Fig. 4e**). An SMLM image reconstructed from high velocity emitters shows a uniformly distributed localization density across the condensate (**Fig. 4f**), while an SMLM image reconstructed solely from low velocity emitters exhibits clusters and nonuniform localization patterns (**Fig. 4g**). This phenomenon is consistent over six condensates where the average excess variance of single-molecule images reconstructed using emitters with low, medium, and high velocities are 0.84 ± 0.33, 0.13 ± 0.06, and 0.05 ± 0.04, respectively (**Fig. 4h**). Condensates imaged using NR show the same trend (**Extended Data Fig. 8**).

NR and NB emitters with longer burst times tend to have lower velocities (**Fig. 4i**). Hubs shown in SMLM images that are reconstructed from longer burst emitters and slowly moving emitters are consistent with one another (**Extended Data Fig. 8**). This correlation suggests the presence of significant physical crosslinking at nanoscale hubs. These high-density crosslinks are likely contributors to the trapping of NR and NB dyes for relatively long periods of time, thus restricting their movements. To ascertain if this interpretation was reasonable, we analyzed the motions of networked chains in the lattice-based simulations of Farag et al., [10]. Specifically, we probed the correlation between molecular displacements and the extent of crosslinking. These simulations show that A1-LCD chains that are part of densely crosslinked networks have smaller overall displacements (**Fig. 4j,** see methods).

Discussion

Overall, the three fluorogenic probes NB, NR, and MC540 sense a broad distribution of chemical environments. Imaging with NB suggests that a relatively uniform hydrophobicity defines the internal environments of A1-LCD condensates. Conversely, inhomogeneities become apparent through hubs that are observed using NR, which suggests that this probe binds preferentially to hubs that are more hydrophobic than the background of the condensate. The inhomogeneities span from tens of nanometers to microns (**Extended Data Fig. 9**). Regions within condensates show up as hubs because they have a greater ability to trap fluorogenic dyes thus providing stable binding sites for them to blink for longer times. In contrast to NB and NR, imaging with MC540 suggests that the interface between dilute and dense phases is a unique environment.

The results reported to this point have focused exclusively on condensates formed by A1-LCD. We also performed single-fluorogen imaging of condensates formed by the RG-rich IDR from the RNA helicase DDX4 [3,33] (**Extended Data Fig. 10**). As with A1-LCD, we found that NB shows relatively uniform fluorescence, NR is concentrated into hubs, and MC540 points to differences in protein properties at the interface versus the interior of condensates.

Overall, our observations of spatially inhomogeneous organizations of molecules affirm recent predictions from computations [10], and provide a structural rationale for reports that condensates formed by low complexity domains are viscoelastic materials [8] with dynamical moduli that have sequence- or architecture-specific relaxation times [7]. The spatial inhomogeneities give condensates a sponge-like appearance. This observation is consistent with inferences made by Handwerger et al., who conjectured, based on quantitative analysis of differential interference microscopy images, that nucleoli, Cajal bodies, and nuclear speckles have sponge-like structures [46].

Many studies of condensate function rely on measurements of partition coefficients and transport properties of small molecules and macromolecules [47-50] that assume a uniform environment within each condensate. Our findings suggest that these measurements must account for the spatial inhomogeneities we have uncovered. The presence of inhomogeneities that span the nanometer to micron scales suggests that partition coefficients are likely to be a distribution of values that are reflective of the size- and chemistry-dependence of preferential partitioning into specific regions within condensates. In addition, there are likely to be preferential interactions that engender inhomogeneities in molecular transport, which one would not expect from a uniformly organized condensate. Clearly, what is required now is an adaptation of the concept of hydrophobicity across multiple length scales [51] and extending inhomogeneous fluid solvation theory to span multiple length scales [52]. This will need to be guided by imaging and tracking of single fluorogenic dyes to probe chemical environments at multiple length scales. Our work represents a first attempt at direct experimental observation of inhomogeneities. Continued development of new dye functionalities [53,54], imaging hardware [55], and analytical tools [56] is needed to uncover the fundamental molecular mechanisms at work within condensates.

Acknowledgments

This work was funded by the Air Force Office of Scientific Research grant (to ASG and RVP), the St. Jude Research Collaborative on the Biology and Biophysics of RNP granules (to RVP), and the National Institutes of Health (F32GM146418-01A1 to MRK and R35GM124858 to MDL).

Author contributions

R.V.P and M.D.L conceived and supervised the research. T.W. designed and performed the imaging experiments and analyzed the data. M.R.K prepared and labeled the A1-LCD and DDX4 proteins, performed phase separation assays, and contributed intellectual insights. M.F. performed the LASSI simulations and his simulations provided the predictive impetus. T.W., M.D.L., and R.V. P. wrote and edited the manuscript with input from all authors.

Competing interests

The authors declare no competing interests.

Additional information

Details of the imaging methods, analysis of images, constructs used, the preparation of condensates, LaSSI simulations, additional data and supplemental figures are presented in the supplementary material.

Correspondence and requests for materials should be addressed to R.V.P. and M.D.L.

1 Lyon, A. S., Peeples, W. B. & Rosen, M. K. A framework for understanding the functions of biomolecular condensates across scales. *Nature Reviews Molecular Cell Biology* **22**, 215-235, doi:10.1038/s41580-020-00303-z (2021).

2 Bremer, A. *et al.* Deciphering how naturally occurring sequence features impact the phase behaviours of disordered prion-like domains. *Nature Chemistry* **14**, 196-207, doi:10.1038/s41557-021-00840-w (2022).

3 Nott, Timothy J. *et al.* Phase Transition of a Disordered Nuage Protein Generates Environmentally Responsive Membraneless Organelles. *Molecular Cell* **57**, 936-947, doi:https://doi.org/10.1016/j.molcel.2015.01.013 (2015).

4 Choi, J.-M., Holehouse, A. S. & Pappu, R. V. Physical Principles Underlying the Complex Biology of Intracellular Phase Transitions. *Annual Review of Biophysics* **49**, 107-133, doi:10.1146/annurev-biophys-121219-081629 (2020).

5 Mittag, T. & Pappu, R. V. A conceptual framework for understanding phase separation and addressing open questions and challenges. *Molecular Cell* **82**, 2201-2214, doi:https://doi.org/10.1016/j.molcel.2022.05.018 (2022).

6 Broadbent, S. R. & Hammersley, J. M. Percolation processes: I. Crystals and mazes. *Mathematical Proceedings of the Cambridge Philosophical Society* **53**, 629-641, doi:10.1017/S0305004100032680 (1957).

7 Alshareedah, I., Moosa, M. M., Pham, M., Potoyan, D. A. & Banerjee, P. R. Programmable Viscoelasticity in Protein-RNA Condensates with Disordered Sticker-Spacer Polypeptides. *Nature Communications* **12**, 6620, doi:10.1101/2021.01.24.427968 (2021).

8 Jawerth, L. *et al.* Protein condensates as aging Maxwell fluids. *Science* **370**, 1317-1323, doi:10.1126/science.aaw4951 (2020).

9 Zhou, H.-X. Viscoelasticity of biomolecular condensates conforms to the Jeffreys model. *The Journal of Chemical Physics* **154**, 041103, doi:10.1063/5.0038916 (2021).

10 Farag, M. *et al.* Condensates formed by prion-like low-complexity domains have small-world network structures and interfaces defined by expanded conformations. *Nature Communications* **13**, 7722, doi:10.1038/s41467-022-35370-7 (2022).

11 Bergeron-Sandoval, L. P. *et al.* Endocytic proteins with prion-like domains form viscoelastic condensates that enable membrane remodeling. *Proceedings of the National Academy of Sciences USA* **118**, e2113789118, doi:10.1073/pnas.2113789118 (2021).

12 Wróbel, J. K., Cortez, R. & Fauci, L. Modeling viscoelastic networks in Stokes flow. *Physics of Fluids* **26**, 113102, doi:10.1063/1.4900941 (2014).

13 Shillcock, J. C., Lagisquet, C., Alexandre, J., Vuillon, L. & Ipsen, J. H. Model biomolecular condensates have heterogeneous structure quantitatively dependent on the interaction profile of their constituent macromolecules. *Soft Matter*, 10.1039/D1032SM00387B, doi:10.1039/D2SM00387B (2022).

14 Espinosa, J. R. *et al.* Liquid network connectivity regulates the stability and composition of biomolecular condensates with many components. *Proceedings of the National Academy of Sciences* **117**, 13238-13247, doi:doi:10.1073/pnas.1917569117 (2020).

15 Molliex, A. *et al.* Phase separation by low complexity domains promotes stress granule assembly and drives pathological fibrillization. *Cell* **163**, 123-133, doi:10.1016/j.cell.2015.09.015 (2015).

16 Franzmann, T. M. *et al.* Phase separation of a yeast prion protein promotes cellular fitness. *Science* **359**, doi:10.1126/science.aao5654 (2018).

17 Wei, M. T. *et al.* Phase behaviour of disordered proteins underlying low density and high permeability of liquid organelles. *Nature Chemistry* **9**, 1118-1125, doi:10.1038/nchem.2803 (2017).

18 Incicco, J. J., Roy, D., Stuchell-Brereton, M. D. & Soranno, A. in *Phase-Separated Biomolecular Condensates: Methods and Protocols* (eds Huan-Xiang Zhou, Jan-Hendrik Spille, & Priya R. Banerjee) 161-198 (Springer US, 2023).

19 Ganser, L. R., Ge, Y. & Myong, S. in *Phase-Separated Biomolecular Condensates: Methods and Protocols* (eds Huan-Xiang Zhou, Jan-Hendrik Spille, & Priya R. Banerjee) 149-160 (Springer US, 2023).

20 Grimm, J. B., Heckman, L. M. & Lavis, L. D. in *Progress in Molecular Biology and Translational Science* Vol. 113 (ed May C. Morris) 1-34 (Academic Press, 2013).

21 Martinez, V. & Henary, M. Nile Red and Nile Blue: Applications and Syntheses of Structural Analogues. *Chemistry – A European Journal* **22**, 13764-13782, doi:https://doi.org/10.1002/chem.201601570 (2016).

22 Verkman, A. S. Mechanism and kinetics of merocyanine 540 binding to phospholipid membranes. *Biochemistry* **26**, 4050-4056, doi:10.1021/bi00387a046 (1987).

23 Li, H. & Vaughan, J. C. Switchable Fluorophores for Single-Molecule Localization Microscopy. *Chemical Reviews* **118**, 9412-9454, doi:10.1021/acs.chemrev.7b00767 (2018).

24 Lew, M. D. *et al.* Three-dimensional superresolution colocalization of intracellular protein superstructures and the cell surface in live Caulobacter crescentus. *Proceedings of the National Academy of Sciences* **108**, E1102-E1110, doi:doi:10.1073/pnas.1114444108 (2011).

25 Spehar, K. *et al.* Super-resolution Imaging of Amyloid Structures over Extended Times by Using Transient Binding of Single Thioflavin T Molecules. *ChemBioChem* **19**, 1944-1948, doi:https://doi.org/10.1002/cbic.201800352 (2018).

26 Danylchuk, D. I., Moon, S., Xu, K. & Klymchenko, A. S. Switchable Solvatochromic Probes for Live-Cell Super-resolution Imaging of Plasma Membrane Organization. *Angewandte Chemie International Edition* **58**, 14920-14924, doi:https://doi.org/10.1002/anie.201907690 (2019).

27 Ding, T., Wu, T., Mazidi, H., Zhang, O. & Lew, M. D. Single-molecule orientation localization microscopy for resolving structural heterogeneities between amyloid fibrils. *Optica* **7**, 602-607, doi:10.1364/OPTICA.388157 (2020).

28 Lu, J., Mazidi, H., Ding, T., Zhang, O. & Lew, M. D. Single-Molecule 3D Orientation Imaging Reveals Nanoscale Compositional Heterogeneity in Lipid Membranes. *Angewandte Chemie International Edition* **59**, 17572-17579, doi:https://doi.org/10.1002/anie.202006207 (2020).

29 Hou, Y., Bardo, A. M., Martinez, C. & Higgins, D. A. Characterization of Molecular Scale Environments in Polymer Films by Single Molecule Spectroscopy. *The Journal of Physical Chemistry B* **104**, 212-219, doi:10.1021/jp992312y (2000).

30 Sackett, D. L., Knutson, J. R. & Wolff, J. Hydrophobic surfaces of tubulin probed by time-resolved and steady-state fluorescence of nile red. *Journal of Biological Chemistry* **265**, 14899-14906, doi:https://doi.org/10.1016/S0021-9258(18)77201-3 (1990).

31 Tajalli, H., Gilani, A. G., Zakerhamidi, M. S. & Tajalli, P. The photophysical properties of Nile red and Nile blue in ordered anisotropic media. *Dyes and Pigments* **78**, 15-24, doi:https://doi.org/10.1016/j.dyepig.2007.10.002 (2008).

32 Martin, E. W. *et al.* Valence and patterning of aromatic residues determine the phase behavior of prion-like domains. *Science* **367**, 694-699, doi:10.1126/science.aaw8653 (2020).

33 Brady, J. P. *et al.* Structural and hydrodynamic properties of an intrinsically disordered region of a germ cell-specific protein on phase separation. *Proceedings of the National Academy of Sciences USA* **114**, E8194-E8203, doi:doi:10.1073/pnas.1706197114 (2017).

34 Sharonov, A. & Hochstrasser, R. M. Wide-field subdiffraction imaging by accumulated binding of diffusing probes. *Proceedings of the National Academy of Sciences* **103**, 18911-18916, doi:doi:10.1073/pnas.0609643104 (2006).

35 Greenspan, P. & Fowler, S. D. Spectrofluorometric studies of the lipid probe, nile red. *Journal of Lipid Research* **26**, 781-789, doi:https://doi.org/10.1016/S0022-2275(20)34307-8 (1985).

36 Kuo, C. & Hochstrasser, R. M. Super-resolution Microscopy of Lipid Bilayer Phases. *Journal of the American Chemical Society* **133**, 4664-4667, doi:10.1021/ja1099193 (2011).

37 Lelek, M. *et al.* Single-molecule localization microscopy. *Nature Reviews Methods Primers* **1**, 39, doi:10.1038/s43586-021-00038-x (2021).

38 Betzig, E. *et al.* Imaging Intracellular Fluorescent Proteins at Nanometer Resolution. *Science* **313**, 1642-1645, doi:doi:10.1126/science.1127344 (2006).

39 Hess, S. T., Girirajan, T. P. K. & Mason, M. D. Ultra-High Resolution Imaging by Fluorescence Photoactivation Localization Microscopy. *Biophysical Journal* **91**, 4258-4272, doi:https://doi.org/10.1529/biophysj.106.091116 (2006).

40 Rust, M. J., Bates, M. & Zhuang, X. Sub-diffraction-limit imaging by stochastic optical reconstruction microscopy (STORM). *Nature Methods* **3**, 793-796, doi:10.1038/nmeth929 (2006).

41 Chhabra, R. Nonwoven Uniformity — Measurements Using Image Analysis. *International Nonwovens Journal* **os-12**, 1558925003os-1551200112, doi:10.1177/1558925003os-1200112 (2003).

42 Ripley, B. D. Modelling Spatial Patterns. *Journal of the Royal Statistical Society: Series B (Methodological)* **39**, 172-192, doi:https://doi.org/10.1111/j.2517-6161.1977.tb01615.x (1977).

43 Khater, I. M., Nabi, I. R. & Hamarneh, G. A Review of Super-Resolution Single-Molecule Localization Microscopy Cluster Analysis and Quantification Methods. *Patterns* **1**, doi:10.1016/j.patter.2020.100038 (2020).

44 Malkusch, S. *et al.* Coordinate-based colocalization analysis of single-molecule localization microscopy data. *Histochemistry and Cell Biology* **137**, 1-10, doi:10.1007/s00418-011-0880-5 (2012).

45 Shen, M. *et al.* Nanoscale Colocalization of Fluorogenic Probes Reveals the Role of Oxygen Vacancies in the Photocatalytic Activity of Tungsten Oxide Nanowires. *ACS Catalysis* **10**, 2088-2099, doi:10.1021/acscatal.9b04481 (2020).

46 Handwerger, K. E., Cordero, J. A. & Gall, J. G. Cajal Bodies, Nucleoli, and Speckles in the Xenopus Oocyte Nucleus Have a Low-Density, Sponge-like Structure. *Molecular Biology of the Cell* **16**, 202-211, doi:10.1091/mbc.e04-08-0742 (2005).

47 Klein, I. A. *et al.* Partitioning of cancer therapeutics in nuclear condensates. *Science* **368**, 1386-1392, doi:doi:10.1126/science.aaz4427 (2020).

48 Banani, S. F., Lee, H. O., Hyman, A. A. & Rosen, M. K. Biomolecular condensates: organizers of cellular biochemistry. *Nature reviews. Molecular cell biology* **18**, 285-298, doi:10.1038/nrm.2017.7 (2017).

49 Banani, S. F. *et al.* Compositional Control of Phase-Separated Cellular Bodies. *Cell* **166**, 651-663, doi:10.1016/j.cell.2016.06.010 (2016).

50 Riback, J. A. *et al.* Composition-dependent thermodynamics of intracellular phase separation. *Nature* **581**, 209-214, doi:10.1038/s41586-020-2256-2 (2020).

51 Lum, K., Chandler, D. & Weeks, J. D. Hydrophobicity at Small and Large Length Scales. *The Journal of Physical Chemistry B* **103**, 4570-4577, doi:10.1021/jp984327m (1999).

52 Huggins, D. J. Application of inhomogeneous fluid solvation theory to model the distribution and thermodynamics of water molecules around biomolecules. *Physical chemistry chemical physics : PCCP* **14**, 15106-15117, doi:10.1039/C2CP42631E (2012).

53 Needham, L.-M. *et al.* ThX – a next-generation probe for the early detection of amyloid aggregates. *Chemical Science* **11**, 4578-4583, doi:10.1039/C9SC04730A (2020).

54 Aparin, I. O. *et al.* Fluorogenic Dimers as Bright Switchable Probes for Enhanced Super-Resolution Imaging of Cell Membranes. *Journal of the American Chemical Society* **144**, 18043-18053, doi:10.1021/jacs.2c07542 (2022).

55 Zhang, O. *et al.* Six-dimensional single-molecule imaging with isotropic resolution using a multi-view reflector microscope. *Nature Photonics*, doi:10.1038/s41566-022-01116-6 (2022).

56 Schröder, T. *et al.* Shrinking gate fluorescence correlation spectroscopy yields equilibrium constants and separates photophysics from structural dynamics. *Proceedings of the National Academy of Sciences* **120**, e2211896120, doi:doi:10.1073/pnas.2211896120 (2023).